Experimental Simulation of High Energy-Density Plasma Interaction with Liquid Metal Media for Inertial Fusion Reactor First Wall Studies

Elijah Martin

North Carolina State University, Department of Nuclear Engineering
Burlington Engineering Laboratory, Raleigh, NC 27695

Abstract

Inertial confinement fusion (ICF) is a promising technology positioned to address the future energy needs of the world. An advanced design concept for ICF reactors is to use a circulating liquid barrier to protect the first wall of the target chamber. With the impaction of the high energy-density plasma on the liquid barrier, sputtering and vaporization can occur causing particulate matter to enter the target chamber interior volume. In order to best engineer the design of the target chamber, this interaction must be well characterized. A small-size experimental facility was designed, constructed, and operated at NC State University to simulate the interaction of high energy-density plasma with liquid metals. This study focuses on characterization of the plasma-liquid metal plume. Characterization of the generated plumes shape and size of evolved vaporized liquid metal particulates; density and other plasma parameters were studied in this research. Electrical and spectral data were obtained for each experiment to obtain the plasma parameters including total power, impedance, electron temperature and density and identification of species. It was determined that a typical plasma generated from a 2 kV discharge has a temperature of 1.0 ± 0.3 eV and a density of 4.2 ± 1.7 x 10^{17} cm^{-3}. The height and geometric configurations of the collection substrates were changed to produce a model of the generated metallic plume. Data analysis of the substrates indicates that the plume has a higher density profile and smaller particulates at distances closer to the point of impact, and the particulate size increases and the particulate density profile decreases with increased distance from liquid metal pool.

Keywords: Inertial confinement fusion, pulsed power, time integrated optical emission spectroscopy

1. Introduction

Plasma interaction with first wall and interior reactor chamber components is an influencing factor in the design of Inertial Confinement Fusion (ICF) facilities. An economical ICF reactor must include a first wall protection scheme, due to the fact that ablation of the interior chamber walls will occur, due to the interactions between the high energy density plasma with interior components. This interaction is severe enough that the frequency and cost of replacing components would outweigh the value of power produced. The concept of a liquid metal wall, in which a circulating lithium curtain would be used, has been considered in many studies. The interaction of plasmas with moving liquid metals is a complex subject due to the influence of hydrodynamics, evaporation and droplet formation, and nucleation and agglomeration of condensed particulates. Due to this complexity, a detailed understanding of this interaction must be known before the liquid first wall protection scheme can be successfully implemented.

The concept of a liquid metal first wall for ICF facilities has been proposed and studied, including the possibility of using a moving liquid metal curtain in the National Ignition Facility (NIF).[1] Although a drywall is highly considered for laser-driven ICF facilities, wetted wall and thick liquid wall are considered more favorable for light and heavy ion drivers.[2,3]

Under the condition of plasma impact on the liquid metal wall, it is expected that high energy-density plasma will sputter the liquid metal, resulting in strong evaporation of particulate matter followed by condensation. In order to better understand the problems associated with liquid metal walls, an experiment was designed, constructed, and operated using an arc-generated plasma source positioned above a liquid metal pool. The experimental simulation of plasma-liquid interaction will be scaled using multiple parameters for comparison to actual ICF reactors, such as NIF. Arc-generated plasmas are adequately sufficient to simulate fast pulse modes of high energy-density plasma generation. Studies on devices generating similar plasmas have shown to have electron temperatures on the order of 1–2 eV and electron densities of 10^{16}-10^{17} cm^{-3}.[4,5] Due to the magnitude of the plasma density, local thermodynamic equilibrium assumptions can be made for highly excited states. Thus, the relative line method and stark broadening mechanisms can be utilized in spectral analysis.[6-8]

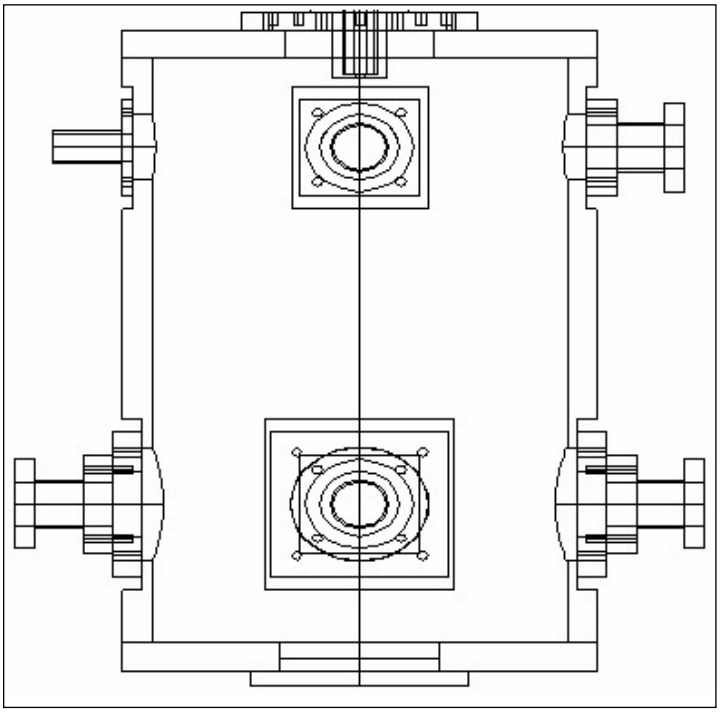

Figure 1. AGEIS chamber

2. Procedure

The experiment was contained in the AGEIS chamber (Arc Generated Explosion Impact on Substrate). The vacuum chamber, shown in Figure 1, is a steel cylinder of diameter 30.5 cm and a height of 60 cm with six radial ports and one axial port which was used for diagnostics, vacuum pumping and electrode feed-through. The chamber was accessed by a flange located at the top of the chamber.

The other ports were used for fiber optic feed-through, vacuum pumping and measurements, and power and electrode feed through. Two cylindrical electrodes with a diameter of 0.6 cm and a length of 25.5 cm were used. A 330 μF, high energy-density capacitor was connected to the cylindrical electrode located at the lower right port and the cylindrical electrode located at the lower left power was connected to ground.

When conducting an experiment, referred to as a "shot", the following steps were taken. Five polished aluminum substrates were cleaned and attached to the exoskeleton. Then a copper fuse 10 cm in length and 0.5 mm in diameter was attached to clamps which were in turn attached to the ends of the electrodes in a fashion indicated by Figure 2. Then the exoskeleton was positioned inside of the vacuum chamber. 150 ± 10 grams of lead were heated to a temperature of 350 ºC and visual confirmation of a phase transition to the liquid state was made. To better simulate the conditions of an inertial confinement fusion reactor, the vacuum chamber was pumped down to 20 ± 2 torr. Finally, the high energy-density capacitor was charged to a potential of 2 kV and the shot was taken. As the high energy-density plasma is generated between the cathode and anode which are attached to the lexan flanges located at the lower left and right ports respectively, the plasma expanded radially and impacted the liquid pool of metal.

An exoskeleton was constructed to fit inside the reaction chamber, this exoskeleton houses the lead reservoir which was moveable allowing the distance between the plasma source and liquid pool of metal to be varied. A heating element placed under the lead reservoir held the temperature at 350 ºC during the experiment. The temperature of the lead reservoir was measured using a thermocouple located between the heating

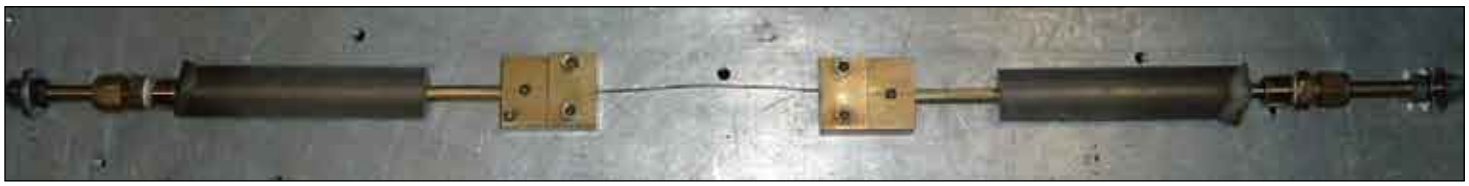

Figure 4. Geometry of electrodes inside the vacuum chamber, shown with copper fuse

element and the steel dish containing the lead reservoir. To collect the plume of metal particulates generated from the plasma impact, five polished aluminum collection substrates 2 cm in diameter were positioned above the plasma source as shown by Figures 3 and 4. The collection substrates were connected to the exoskeleton in such a way that the distance from the lead reservoir could be varied.

The collection substrates were positioned with a geometry to allow for a mirror plane of reflection located at the vertical center plane of the discharge. The discharge current was acquired by a 1:1000 Pearson coil; the discharge voltage was acquired by a 1:1000 Tektronix Capacitively-coupled HV probe. A Tektronix TDS 2024/200 MHz four-channel digital storage oscilloscope was used for data acquisition and storage. An Ocean Optics HR2000 spectrometer was used to obtain emission spectrum from the discharge. The grating of the spectrometer has 600 lines/mm and was blazed at 500 nm, the spectrometer has a resolution of 0.4 nm and a bandwidth ranging from 300 to 730 nm. The emission spectrum of the discharge was obtained using a 100 μm fiber optic, positioned such that a radial view of the expanding plasma was obtained. The 100 μm fiber optic was connected outside the vacuum chamber to a bifurcated 400 μm insulated patch cord that interfaced with the spectrometer and a monochromator attached to a Photomultiplier Tube (PMT).

Figure 3. Geometry of the collection substrates attached to the exoskeleton

Figure 4. Exoskeleton inside of the vacuum chamber

3. Results and Discussion

3.1 Electrical Waveforms

To determine the power dissipated within the high energy-density plasma and the impedance of the plasma, current and voltage waveforms were obtained. Figure 5 depicts typical discharge current and voltage waveforms.

The impedance of the discharge was calculated from Ohms Law. Figure 6 shows the plasma impedance as a function of time for a typical discharge.

Figure 5 shows that the equivalent circuit of the device was underdamped. It was assumed that the plasma had recombined when the voltage dropped to zero, roughly at time t=40 μsec, as shown by Figure 5. Confirmation of this assumption was made from energy conservation and the PMT waveform shown in Figure 7. The net input energy into the discharge was calculated from the difference between the initial and residual energy on the capacitor after the shot. The net input energy was also calculated by integrating the power dissipated within the plasma, shown in Figure 8, over the time length 0 to 40 μsec. From a comparison of both methods used to calculate the net input energy, it was confirmed that discharge was identified by when the voltage dropped to zero.

The net input energy into the plasma was averaged over all shots. On an average, the net input energy was 660 ± 0.6 J. The discharge conditions were constant so that all shots maintained the same net energy input to the system.

To determine when initial breakdown of the discharge occurred, the waveform generated by the PMT was analyzed. It was assumed that initial breakdown occurred when photon emission occurred. A monochromator was used to collect photons resulting from a neutral copper atom electronic transition at 521.8 nm.

Figure 7 shows that breakdown occurred after the initial voltage spike; Figure 7 also indicates that photon emission has terminated when the voltage drops to zero confirming the plasma recombination assumption. It was determined that pickup from the electromagnetic field generated from the shot was distorting the waveform of the PMT. Due to the above fact, an isolation transformer was used to supply AC voltage to all electrical equipment.

3.2 Time Integrated Optical Emission Spectroscopy

To determine the electron temperature of the discharge, the relative line method was utilized.[6-8] It can be shown by equilibrium quantum statistics and thermodynamics that the local thermodynamic equilibrium (LTE) distribution over the state of an atom obeys the following.[6]

$$\frac{N_m}{N} = \frac{g_m}{Z_a(T)} e^{-\frac{E_m}{kT}} \quad (1)$$

Where N_m is the population of state m, N represents the number of same species atoms, g_m is the statistical weight of the upper level energy state m, $Z_a(T)$ represents the partition function, E_m is the upper level energy of state m, and kT is the electron temperature. The ratio of two bound states, m_1 and m_2, can be determined from Equation 1.

$$\frac{N_{m_1}}{N_{m_2}} = \frac{g_{m_1}}{g_{m_2}} e^{-\left[\frac{E_{m_1} - E_{m_2}}{kT}\right]} \quad (2)$$

The integrated emission line intensity, i_{nm}, can be found by integrating the intensity of a transition, I_{nm}, with respect to the angular frequency, ω, along the line of sight in the plasma, L.

$$i_{nm} = \int I_{nm}(\omega) d\omega \quad (3)$$

The assumption was made that the plasma is homogenous along the line of sight.

$$i_{nm} = \frac{h\omega_{nm}}{4\pi} A_{nm} N_m L \quad (4)$$

The angular frequency associated with the transition m → n is represented by ω_{nm}, the transition probability for the transition m → n is represented by A_{nm}, and h represents Planck's constant. A ratio of the integrated emission line intensity, R,

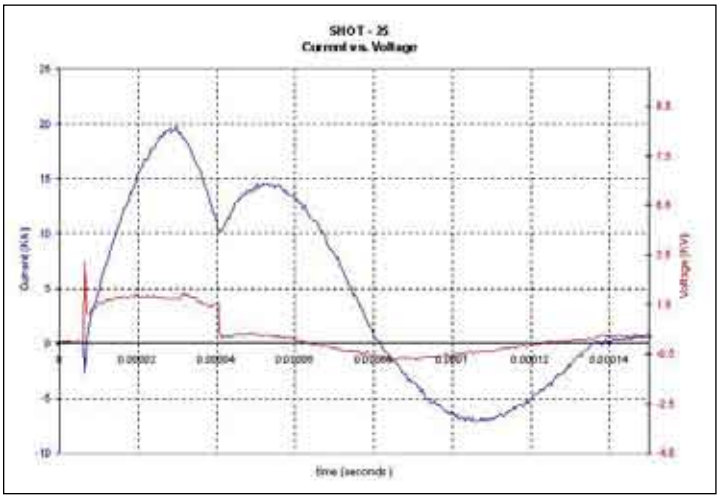

Figure 5. Current and voltage trace of a typical discharge

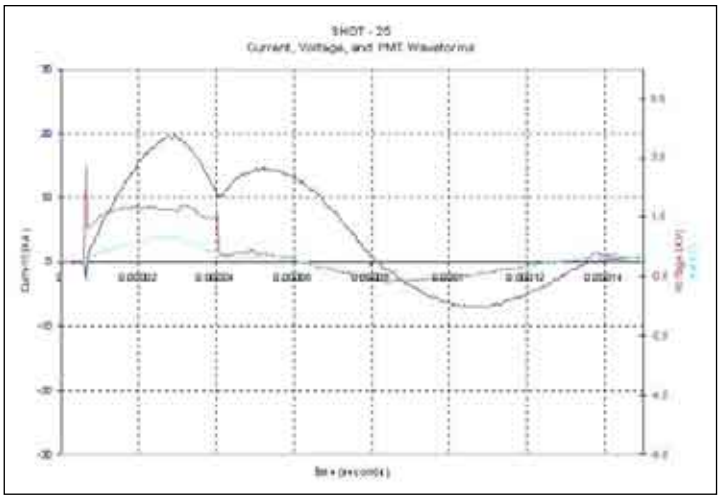

Figure 7. PMT waveform

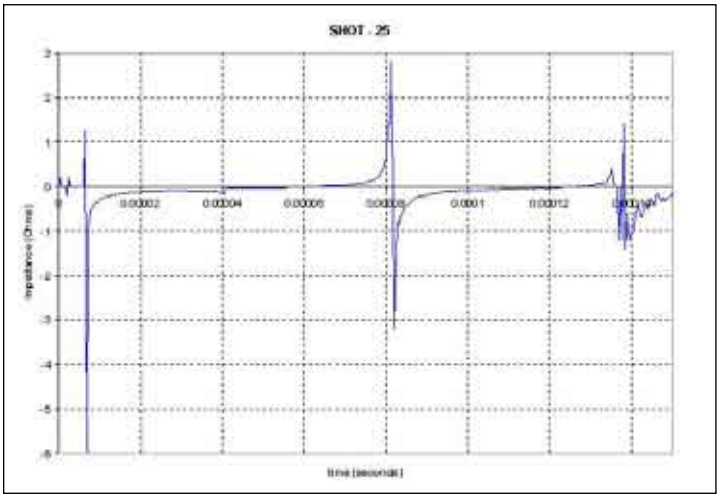

Figure 6. Transient plasma impedance

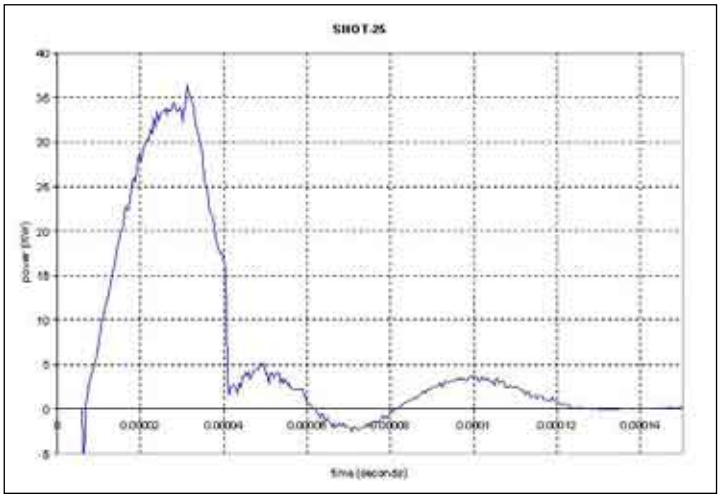

Figure 8. Transient power dissipated into the plasma

given by Equation 5 is taken for transitions $m_1 \rightarrow n_1$ and $m_2 \rightarrow n_2$.

$$R = \frac{i_{n_1 m_1}}{i_{n_2 m_2}} = \frac{w_{n_1 m_1} A_{n_1 m_1} N_{m_1}}{w_{n_2 m_2} A_{n_2 m_2} N_{m_2}} \quad (5)$$

Equation 2 is substituted into equation 5 to giving the following.

$$R = \frac{w_{n_1 m_1} A_{n_1 m_1} g_{m_1}}{w_{n_2 m_2} A_{n_2 m_2} g_{m_2}} e^{\left[\frac{E_{m_1} - E_{m2}}{K T}\right]} \quad (6)$$

The electron temperature, kT, of Equation 6 can be explicitly solved for giving the following expression.

$$k T = \frac{E_{m_2} - E_{m_1}}{h\left[\frac{w_{m_2 n_2} g_{m_2} A_{n_2 m_2}}{w_{m_1 n_1} g_{m_1} A_{n_1 m_1}} R\right]} \quad (7)$$

Equation 7 states that given the ratio of integrated emission line intensity of two bound transitions taking place within the same species atom, the free electron temperature can be determined.

$$l n\left[\frac{i_{n m}}{w_{m n} A_{n m} g_m}\right] = -E_m \frac{1}{k T} + l n\left[\frac{N L h}{Z_a(T)}\right] \quad (8)$$

For LTE transitions of the same species atom the second term on the right hand side of Equation 8 is constant, the first term on the right hand side of Equation 8 is know as the Boltzmann function. The electron temperature can be determined from a plot of the Boltzmann function vs. upper level energy of the transition. Equation 8 was used to determine the electron temperature for the arc-generated plasmas of the AGEIS device. Due to the fact that the use of Equation 8 requires LTE of the excited states used, the LTE state of the discharge must be confirmed. Highly excited states of similar discharges generated by Dale *et al.* and Sharpe *et al.*[4,5] have found to meet the LTE condition. To confirm the LTE assumption, a limit on the principal quantum number of a transition in LTE is given by Fujimoto.[7]

$$p \geq \frac{118}{\Theta^{0.43}} + \frac{2.2 \cdot 10^3}{h^{0.15}} \quad (9)$$

$$\Theta = \frac{T_e}{z^2} \quad (10)$$

$$h = \frac{n_e}{z^7} \quad (11)$$

The electron temperature in Kelvin is represented by T_e, the electron density in m^{-3} is represented by n_e, and z represents the atomic number of the plasma species. Sharpe and Merrill *et al.*[5] reported electron temperatures of 1 to 2 eV and electron densities on the order of 10^{17} cm^{-3} obtained in similar arc-generated discharges. Assuming the plasma parameters will be similar in AGEIS, the lower limit on the principal quantum number, found using Equation 9, was in the range of 50 to 60. Numerical calculations given by Fujimoto have shown that for the given discharge conditions Equation 9 will over predict the lower limit of the principal quantum number by about one half. The lower limit on the principal quantum number for LTE transitions will be assumed to be 25 to 30. It should be noted that Equation 9 is for hydrogen like ions. The calculation conducted here is an approximation. LTE confirmation will be concluded from the linearity of the Boltzmann plot given by Equation 8. Figure 9 depicts a spectrum obtained from a typical discharge.

The following first order neutral copper lines, given in Table 1, were identified in the spectra obtained from typical discharges of AGEIS, the lines are shown with the various constants associated with the transition.[9]

To determine the line integrated emission intensity necessary for use of Equation 8, Peakfit v4.12 was used to provide a numerical integration and other parameters such as the Full Width at Half Maximum (FWHM) of the spectral lines. Figure 10 represents a fitted emission spectrum obtained from a typical discharge of AGEIS.

It was found that the profile of the spectral lines obtained from copper discharges in AGEIS have a Lorentzien profile. Equation 8 was plotted using the identified lines and constants given in Table 1. The electron temperature was determined from the slope of Figure 11.

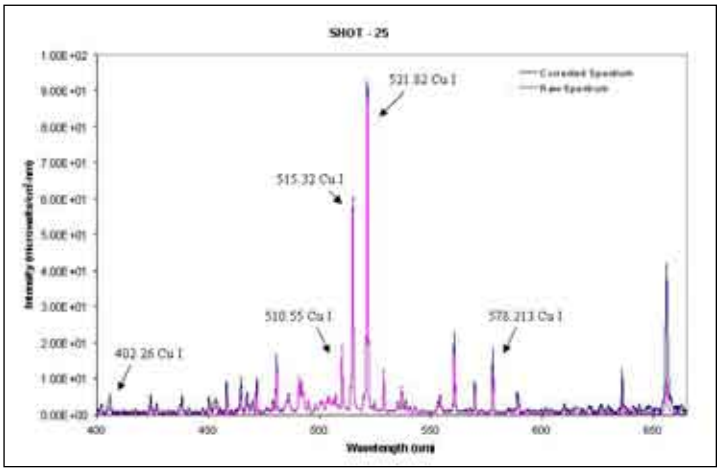

Figure 9. Emission spectra of copper discharge in AGEIS

The linearity of the Boltzmann plot shown in Figure 11 indicates that the transitions associated with the identity lines are in LTE. The electron density, in units of m^{-3}, of the discharge is determined from pressure broadening, also known as Stark broadening, of the neutral copper spectral lines identified above by the following expression.

$$n_e = \frac{FWHM}{w_m} \cdot 10^{23} \qquad (12)$$

The Stark width, ω_m, is a function of electron density and a weak function of electron temperature; Stark width values are obtained for an electron temperature of 10000 K and electron density of 10^{23} m^{-3}. Table 2 gives Stark width values for the identified lines.

The electron temperature and density were determined by the above methods for all discharges, Table 3 gives the calculated values for each discharge.

3.3 Collection Substrates

Digital pictures of the surface of the collection substrates were taken prior and post shot for all substrates, using an Olympus BH2-UMA optical microscope at 100x magnification. The digital pictures were analyzed using ImageJ, a NIH program.[10] ImageJ produces information (in pixel units) on the particle count, average particle size, total area, and area fraction for the digital images. For each substrate 5 pictures were taken at different locations to obtain better averaging. The collection substrates are labeled 1 through 5 in the Tables 4 and 5, where substrate 3 is positioned over the center of the lead reservoir.

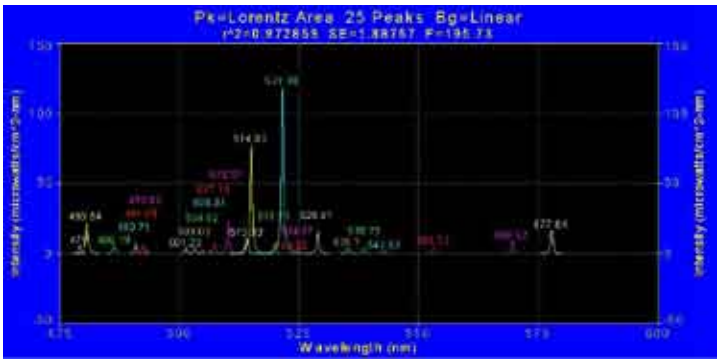

Figure 10. Fitted spectra

Figure 12 shows an original digital image, which is gray scaled and masked by ImageJ.

Due to the fact that the image is gray scaled for analysis by ImageJ, no differentiation between copper and lead particles or the lines occurring on the aluminum surface from the milling process could be determined. To account for this, background images were obtained for aluminum substrates alone and for a case when the lead pool was not present. The size of the aluminum only particles was largely due to the fact that the lines on the surface were not broken by any particulates and therefore appeared as large particles. Although this is not very accurate, it gives an estimate of the background counts and size. For the copper background, more data needs to be taken to accurately define the distribution for a copper only shot.

Preliminary data analysis conducted using ImageJ generally indicates the following trend: the lead particulate plume has a higher density profile and smaller particulates at distances closer to the point of impact with lead reservoir, and the particulate size increases and the particulate density profile decreases with increased distance from the lead reservoir. The particulate size is generally larger on substrates 1 and 5; the particulate density is generally larger on substrates 2 and 4. The particulate density can be correlated to the particulate size from the effect that masking plays in the low-density regions with the larger particle size. This masking effect occurs due to the fact that larger particulates will decrease the area for the smaller particulates to be observed or obscure the viewing of the smaller particulates that are under or on the larger particulates. More data is needed

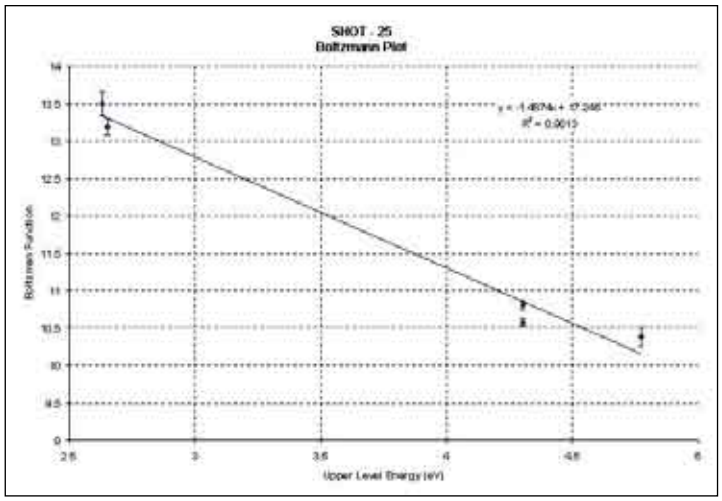

Figure 11. Boltzmann plot of identified lines

Wavelength (nm)	A_{nm} - Transition Probability (10^{-8} s^{-1})	g_m - Statistical Weight	E_m - Upper Level Energy (eV)
402.263	1.90E-01	4	4.773
510.554	2.00E-02	4	2.653
515.324	6.00E-01	4	4.303
521.82	7.50E-01	6	4.304
578.213	1.65E-02	2	2.631

Table 1. First order neutral copper lines present in emission spectra

for a full statistical analysis on the collected plume particulates but from preliminary data analysis, trends are observed in the plume.

4. Conclusions

An experiment designed to generate an arc-driven plasma which will interact with a liquid metal pool has been constructed and tested for operation. It was determined by time integrated optical emission spectroscopy that the discharge average electron density is 4.2 ± 1.7 x 10^{17} cm^{-3} and the average electron temperature is 1.0 ± 0.3 eV. All discharges were established with a net input energy of 660 ± 0.6 Joules. Analysis of collection substrates using ImageJ indicates that the interaction of the high energy-density plasma with the liquid lead reservoir leads to the generation of a lead particulate plume. Nucleation and condensation mechanisms were found to dominate in the plume as the distance from the point of impact is increased; this conclusion is supported by the following trend: the particulate size increases and particulate density decreases as the distance between the collection substrate and the lead reservoir increases. Preliminary data shows that the condensate has a high particulate density core with smaller particulate matter; as the distance from the core is increased, the particulate density decreases, and the particulate size increases. The above conclusions indicate that nucleation and condensation takes place close to the point of impact, 6-7 cm, thus hindering small particulate matter from entering the interior volume of the ICF reactor chamber. Particulate density was shown to decrease as the distance from the point of impact is increased. This effect will lower the coupling between the mechanisms (laser/ion beams) used to drive the fusion reactions, and the plume generated from the interaction of the high energy-density plasma and the liquid first wall.

Wavelength (nm)	ω_d - Stark Width (nm)
402.263	0.431
510.554	4.30E-02
515.324	0.19
521.82	0.22
578.213	7.20E-02

Table 2. Stark width values for various neutral copper lines

Experiment	Temperatue (eV)	Density (cm^{-3})	Net Energy Input (J)
SHOT-1	0.939	1.14E+18	659.9
SHOT-6	1.17	2.8E+17	659.7
SHOT-7	1.15	4.87E+17	659.2
SHOT-8	0.819	2.37E+17	666.4
SHOT-9	0.947	2.76E+17	666
SHOT-10	0.639	1.66E+17	659.6
SHOT-11	1.29	3.2E+17	666.4
SHOT-12	0.701	3.03E+17	659.9
SHOT-14	0.985	3.43E+17	659.9
SHOT-15	0.943	2.51E+17	659.9
SHOT-16	0.661	3.11E+17	660
SHOT-17	0.69	2.16E+17	659.9
SHOT-18	0.663	2.08E+17	659.9
SHOT-36	0.817	5.72E+17	659.6
SHOT-38	0.948	2.83E+17	659.7

Table 3. Electron density and temperature values

Acknowledgements

The author greatly thanks Dr. Mohamed A. Bourham of the Nuclear Engineering Department of North Carolina State University for his countless hours of mentoring and numerous discussions, without his guidance this project would not have been possible. This research was conducted at North Carolina State University to aid the development of an economical power producing inertial confinement fusion reactor.

Collection Substrate	1	2	3	4	5
SHOT-12	4.607	3.392	7.149	2.245	8.189
SHOT-14	4.275	1.783	3.404	3.673	4.669
SHOT-15	4.196	0.759	1.745	2.716	3.042
SHOT-19	1.088	0.588	0.647	0.851	1.015
SHOT-16	9.207	6.948	6.514	3.243	7.892
SHOT-17	5.504	4.408	8.787	10.06	13.08
SHOT-18	2.743	2.25	1.222	6.167	4.909

Table 5. Average particulate size in 1x10^{-2} mm^2

Collection Substrate	1	2	3	4	5
SHOT-12	30.33	32.79	25.21	37.79	17.26
SHOT-14	25.35	92.66	49.5	65.03	45.02
SHOT-15	59	164	88.51	101.8	65.31
SHOT-19	197.3	238.7	84.13	178.7	93.55
SHOT-16	33.38	18.98	18.43	33.02	17.4
SHOT-17	19.43	24.07	14.74	13.12	12.7
SHOT-18	19.86	51.79	58.28	14.09	33.65

Table 6. Particulate surface density in mm^{-2}

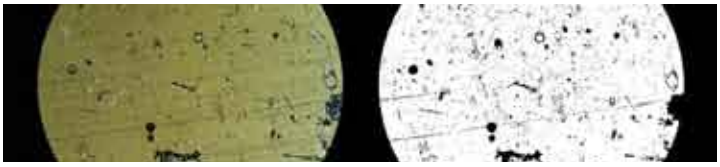

Figure 15. Original (left) and analyzed (rght) picture

References

[1] Moses, E.I. The National Ignition Facility: Status and Plans for the Experimental Program. *Fusion Science and Technology* **2003**, *44*, 11-18.

[2] Meier, W. R.; Raffray, A. R.; Abdel-Khalik, S. I.; Kulcinski, G. L.; Latowski, J. F.; Najmabadi, F.; Olson, C. L.; Peterson, P. F.; Ying, A.; Yoda, M. IFE Chamber Technology - Status and Future Challenges. *Fusion Science and Technology* **2003**, *44*, 27-33.

[3] Moir, R.W.; Bieri, R.L.; Chen, X.M.; Dolan, T.J.; Hoffman, M.A.; House, P.A.; Leber, R.L.; Lee, J.D.; Lee, Y.T.; Liu, J.C.; Longhurst, G.R.; Meier, W.R.; Peterson, P.F.; Petzoldt, R.W.; Schrock, V.E.; Tobin, M.T.; Williams, W.H. HYLIFE-II: A Molten-Salt Inertial Fusion Energy Power Plant Design – Final Report. *Fusion Technology* **1994**, *25*, 5-25

[4] Dale, G.E.; Bourham, M.A. Experimental Investigation into Melt-Layer Erosion of Plasma-Facing Materials. *Fusion Technology* **1998**, *34*, 901-907.

[5] Sharpe, J.P.; Merrill, B.J.; Petti, D.A.; Bourham, M.A.; Gilligan, J.G. Modeling of Particulate Production in the SIRENS Plasma Disruption Simulator. *Journal of Nuclear Materials* **2001**, *290*, 1128-1133.

[6] Griem, H. R. *Principles of Plasma Spectroscopy*; Cambridge University Press: Cambridge, 1997.

[7] Fujimoto, T. *Plasma Spectroscopy*; Oxford University Press: Oxford, 2004.

[8] Hutchinson, I. H. *Principles of Plasma Diagnostics*; Cambridge University Press: Cambridge, 2002.

[9] *CRC Handbook of Chemistry and Physics*. CRC Press, Boca Raton, FL, 76th edition, 1996.

[10] Image processing software package free downloads from NIH, http://rsb.info.nih.gov/ij/index.html.

About the Author

Elijah Martin

Elijah Martin is a fourth year student at North Carolina State University majoring in Physics, Nuclear Engineering, and Chemistry. He has been involved with various research projects involving plasma physics since his freshman year. His primary research interest included optical emission spectroscopy diagnostic techniques, electrical probe techniques, and magnetic confinement fusion.